ELSEVIER

Polymer Vol. 37 No. 5, pp. 831–836, 1996

0032-3861/96/$15.00+0.00

Structure and deformation behaviour of a vinylidene fluoride–tetrafluoroethylene–hexafluoropropylene terpolymer

H. Freimuth, C. Sinn and M. Dettenmaier*
MPI für Polymerforschung, Postfach 3148, D-55021 Mainz, Germany
(Received 30 August 1994; revised 15 December 1994)

The statistical terpolymer composed of 52 mol% vinylidene fluoride (VDF), 36 mol% tetrafluoroethylene (TFE) and 12 mol% hexafluoropropylene (HFP) is a ductile material that can be highly deformed in uniaxial tensile tests. Wide-angle and small-angle X-ray scattering (WAXS, SAXS) techniques have been used to study the structure of uniaxially oriented samples. WAXS shows that the terpolymer exhibits a low degree of crystallinity ($x_c \approx 0.1$). The crystalline structure combines features of both VDF and TFE, in agreement with previous studies on VDF/TFE copolymers. Concentration fluctuations do not contribute significantly to SAXS of the VDF/TFE/HFP melt. Melt-crystallized samples exhibit a lamellar morphology with a long period of $L = 12$ nm and a volume fraction of crystallites of $\Phi_c = 0.26$. Deformation of the terpolymer at $T = 50$°C results in a four-point SAXS pattern, which gradually changes to a two-point pattern when the drawing temperature increases. The mean-square fluctuation of the electron density strongly decreases at low drawing temperatures. It is assumed that vacancies introduced near the grain boundaries reduce the density of the crystalline layers.

(Keywords: fluorinated terpolymers; morphology; deformation)

INTRODUCTION

Terpolymers containing vinylidene fluoride (VDF), tetrafluoroethylene (TFE) and hexafluoropropylene (HFP) have received commercial interest because of their chemical resistance, thermal stability, processability and optical properties. Among other applications, they have been used in optical fibres as cladding material with low refractive index[1]. Many physical properties that are relevant to technological applications are affected by the structure of the material. This article focuses on the structure of isotropic and uniaxially oriented samples of VDF/TFE/HFP as revealed by wide-angle and small-angle X-ray scattering (WAXS and SAXS).

Lovinger *et al.*[2–5] and other groups[6–10] (see also ref. 11 for review) have extensively investigated the crystalline structure of both VDF/TFE and VDF/trifluoroethylene (TrFE) copolymers in connection with the ferroelectric–paraelectric phase transition that occurs in these materials at sufficiently high VDF content. The interchain lattice constants increase as the bulkier TFE and TrFE units replace the VDF ones. Both copolymer systems exhibit a high degree of crystallinity ($x_c \approx 0.7$–0.8) over the whole concentration range. On the other hand, the incorporation of the even bulkier HFP units reduces the degree of crystallinity of polytetrafluoroethylene (PTFE)[12,13] and more drastically that of poly(vinylidene fluoride) (PVDF)[14]. Less attention has been given to the morphology of the copolymers. Bourgaux-Leonard *et al.*[8,10] have investigated VDF/TrFE copolymers that exhibit a ferroelectric–paraelectric phase transition. They observed pronounced changes in the degree of crystallinity and the lamellar morphology during temperature cycling through the Curie transition.

From the mechanical data compiled in the literature (see e.g. ref. 15), it is well known that copolymers containing VDF, TFE and HFP are ductile materials that can be stretched to high extension ratios. However, little information is available on the structural changes that are produced by the deformation of the copolymers. Studies on oriented samples have frequently been performed with the objective to facilitate the structural interpretation of WAXS data. The deformation history and the morphology of these samples are generally not discussed in detail.

EXPERIMENTAL

The statistical terpolymer (supplied by Hoechst AG) was synthesized by aqueous emulsion polymerization and consisted of 52 mol% VDF, 36 mol% TFE and 12 mol% HFP. The samples used in these studies were prepared from granular material, which was compression moulded at $T = 175$°C and then quenched in ice–water. The thermal behaviour of the samples was studied by d.s.c. using Perkin-Elmer DSC 7. Measurements performed at a heating rate of 10°C min^{-1} revealed a glass transition temperature, $T_g = 3$°C and a broad melting range with a peak situated at 120°C. Dynamic mechanical measurements under torsion were carried out with a Rheometrics mechanical spectrometer (model 800) operated at a frequency of 10 rad s^{-1}. Tensile tests with an Instron

* To whom correspondence should be addressed

machine were performed at a nominal strain rate of $6 \times 10^{-4}\,s^{-1}$. X-ray scattering experiments were carried out using nickel-filtered Cu K_α radiation. A Siemens diffractometer and a Kratky camera covered the wide-angle and small-angle range, respectively. SAXS data of isotropic samples measured with the Kratky camera were corrected for slit collimation[16]. Absolute measurements were performed by using a Lupolen standard. A beam line equipped with a rotating anode and a two-dimensional detector provided supplementary information on the anisotropic scattering patterns of oriented samples.

RESULTS AND DISCUSSION

Deformation behaviour

Figure 1 shows the viscoelastic behaviour of the VDF/TFE/HFP terpolymer as a function of temperature. Dynamic mechanical measurements performed in torsion reveal two relaxation mechanisms. The relaxation at low temperatures is observed in the same temperature range as the γ-relaxation of PVDF (see e.g. ref. 11) and PTFE[12,13]. There is strong evidence that this relaxation results from local chain motions in the amorphous regions[17,18]. The relaxation at high temperatures is associated with a change in the storage modulus by one decade and occurs at a temperature close to T_g measured by d.s.c. The identification of this relaxation with the glass transition is supported by the fact that PVDF[11] and PTFE[12] exhibit relaxations at a lower and higher temperature, respectively, which are both attributed to cooperative chain motions in the amorphous regions.

Figure 2 shows the stress–strain behaviour of the terpolymer as a function of temperature. The results are typical for a ductile polymer that deforms by shear yielding. However, the intensive stress-whitening of the sample stretched at $T = 20°C$ indicates the existence of a cavitational mode of plasticity at temperatures close to T_g.

Structure as revealed by WAXS

Figure 3 shows the wide-angle diffractogram of an undeformed sample, which exhibits two amorphous halos at $q = 12.4 \pm 0.2\,nm^{-1}$ and $q = 27.5 \pm 0.3\,nm^{-1}$ ($q = (4\pi/\lambda)\sin(\theta/2)$). A single Bragg reflection is superimposed on the first halo at $q = 12.89 \pm 0.05\,nm^{-1}$. A degree of crystallinity of $x_c = 0.1$ has been estimated from the ratio of the integrated intensities under the Bragg reflection and the first halo. *Figure 4* shows the

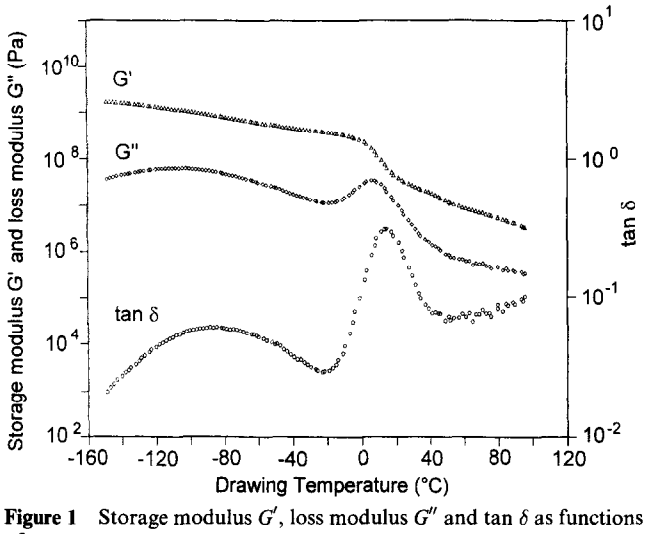

Figure 1 Storage modulus G', loss modulus G'' and tan δ as functions of temperature

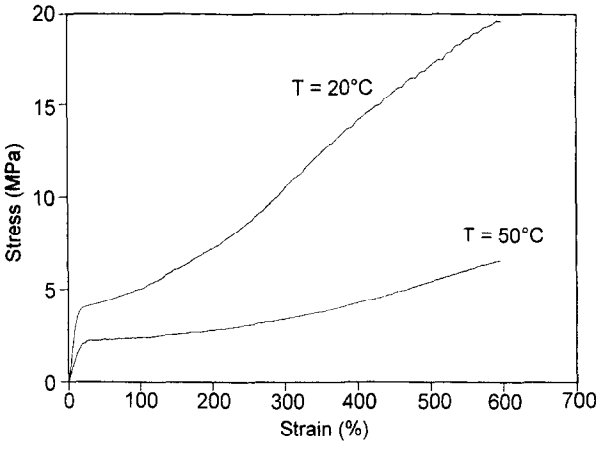

Figure 2 Stress–strain behaviour at $T = 20°C$ and $T = 50°C$

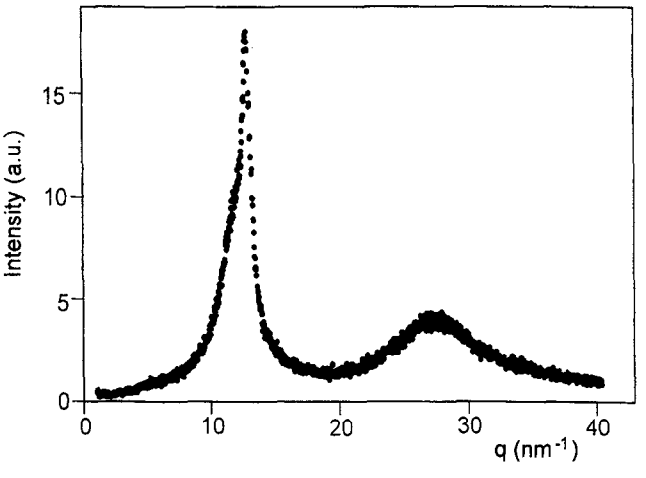

Figure 3 Wide-angle diffractogram of an undeformed sample

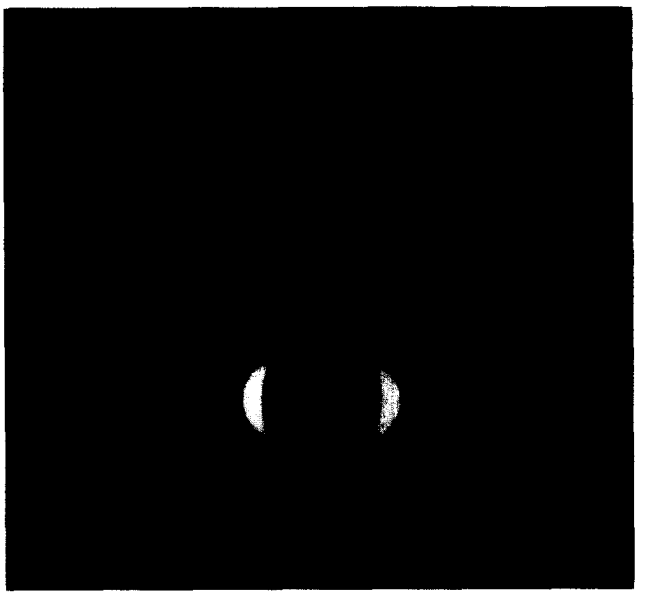

Figure 4 WAXS pattern of a sample stretched at $T = 100°C$ to $\alpha = 4.5$. The draw axis is vertical

WAXS pattern of a sample stretched at $T = 100°C$ to an extension ratio of $\alpha = 4.5$. The Bragg reflection of the oriented sample concentrates on the equator, indicating Miller indices of the type (h k 0). A closer inspection of the WAXS pattern reveals two meridional reflections (00l) with positions at $q = 24.7 \pm 0.1\,nm^{-1}$ and $q = 49.3 \pm 0.2\,nm^{-1}$. The small number of reflections excludes a detailed structural analysis of the unit cell. Under these conditions, information on the structure of homo- and copolymers that are chemically related to the VDF/TFE/HFP terpolymer may be useful to interpret the WAXS data. In fact, there is strong evidence that the crystalline structure of the terpolymer combines features of both PTFE and PVDF. In the high-temperature phase, designated phase I, the molecular packing of PTFE is metrically hexagonal with an inter-axial nearest distance of $a = 566\,pm$[5,19–22]. Both the high intensity and the Bragg spacing of the equatorial reflection in the fibre pattern of the terpolymer indicate the same type of molecular packing as observed for PTFE. In fact, the Bragg spacing of this reflection assigned as (1 0 0) yields $a = 563 \pm 1\,pm$, which is close to the value reported for PTFE, indicating that the packing of the terpolymer chains is governed by the bulky TFE units. In phase I, the molecules of PTFE adopt a 15/7 helical conformation[19–22]. However, the terpolymer, like PVDF in the β-phase[5,23–25], crystallizes in a 2/1 planar *trans-trans* conformation, as revealed by the exact meridional reflections assigned as (0 0 1) and (0 0 2). The (0 0 1) reflection, which is only observed because the hexagonal packing of the copolymer chains exhibits high longitudinal disorder, has a Bragg spacing of $c = 254 \pm 1\,pm$ as compared to $c = 256\,pm$ for PVDF[5].

The crystalline structure of the terpolymer has been studied as a function of drawing temperature, T. The inter-axial nearest distance, a, increases from $a = 563\,pm$ at $T = 100°C$ to $a = 572\,pm$ at $T = 50°C$ whereas c remains approximately constant. There is no evidence for the existence of a second (ferroelectric) phase as observed for VDF/TrFE copolymers[8,10].

The values of a and c obtained for the VDF/TFE/HFP terpolymer are in good agreement with data that Lovinger *et al.*[5] reported for VDF/TFE copolymers with less than 35 mol% VDF. However, the terpolymer exhibits a much lower degree of crystallinity. In fact, the value of $x_c = 0.1$ is close to that measured for VDF/HFP copolymers[14] with the same mole fraction of HFP units, whereas VDF/TFE copolymers exhibit a high degree of crystallinity ($x_c = 0.7$–0.8) over the whole concentration range[5]. This result indicates that the incorporation of HFP units into the VDF/TFE copolymers does not appreciably affect the crystalline structure, but does, however, strongly reduce the degree of crystallinity.

Structure as revealed by SAXS

Figure 5 shows the desmeared SAXS curve of an isotropic VDF/TFE/HFP sample. I is defined as the ratio of the scattering intensity per unit volume of the sample to that of a single electron. The peak in the scattering curve clearly reflects the periodic arrangement of crystalline and amorphous regions in stacks of lamellae. The Lorentz-corrected scattering curve included in *Figure 5* exhibits a peak maximum at $q = 0.52 \pm 0.01\,nm^{-1}$ corresponding to a long period, $L = 12.0 \pm 0.4\,nm$ (see also *Table 1*). For the subsequent analysis of the SAXS

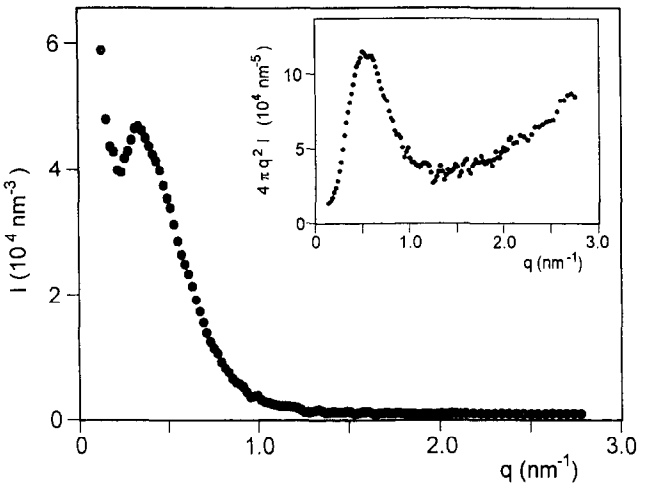

Figure 5 Desmeared SAXS curve of an undeformed sample. The Lorentz-corrected scattering curve is included

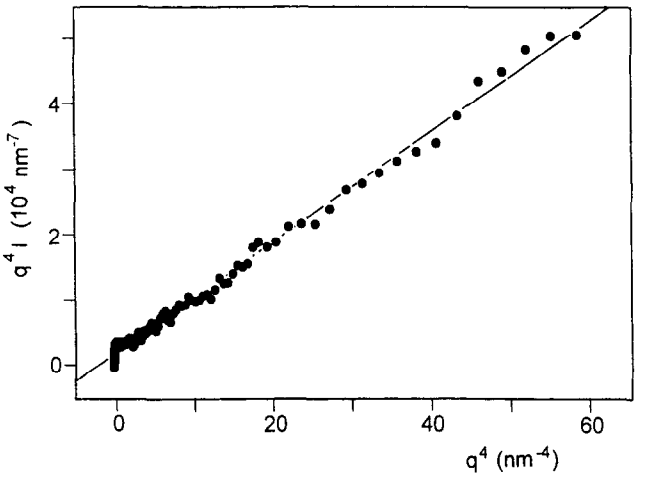

Figure 6 Kratky plot of the desmeared SAXS of an undeformed sample

data, it is important to focus on the scattering behaviour at high values of q. The Kratky plot shown in *Figure 6* demonstrates that the scattering intensity per unit volume, I obeys for $q \to \infty$ the asymptotic law:

$$I = A/q^4 + B \qquad (1)$$

where A and B are constants. The first term is typical for a two-phase system with sharp phase boundaries[26]. The second term must be attributed to fluctuations of the electron density within the amorphous regions. In the case of copolymers consisting of units with different electron densities, these fluctuations may result from fluctuations of both density and concentration. In the limit of small values of q, the scattering from thermal density fluctuations is given by[27]:

$$I = \rho_e^2 \kappa_t k T \qquad (2)$$

where ρ_e is the average electron density, κ_t is the isothermal compressibility, k the Boltzmann constant and T the temperature. The value of κ_t of the VDF/TFE/HFP melt has been measured as a function of temperature. As shown in *Figure 7*, the SAXS intensities, I, calculated from κ_t according to equation (2) fall only slightly below the experimental data, indicating that

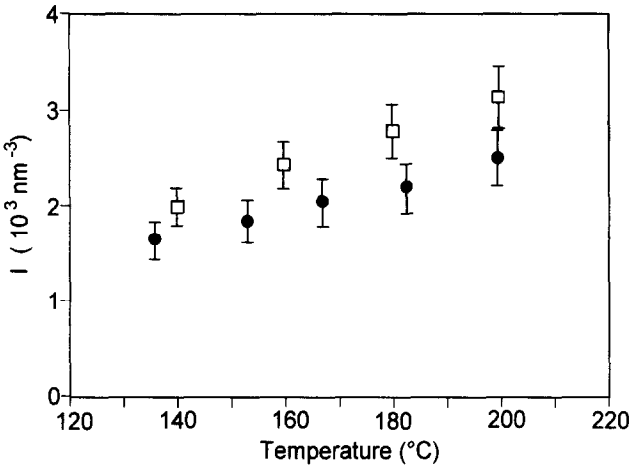

Figure 7 SAXS of the melt as a function of temperature: (□) data derived from the desmeared SAXS curve for $q \rightarrow 0$; (●) data calculated from equation (2)

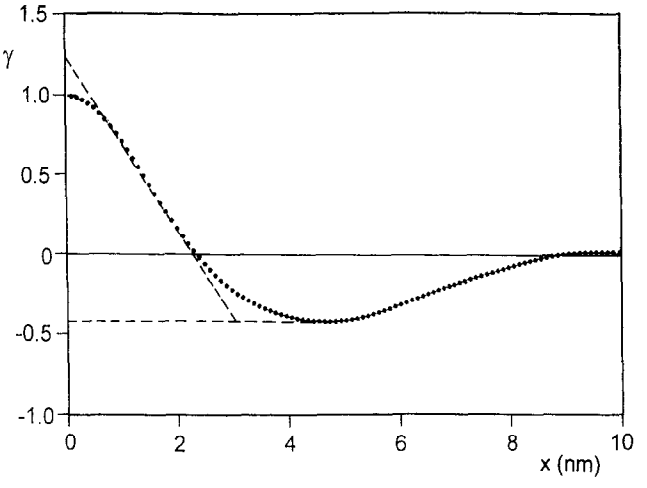

Figure 8 Correlation function of an undeformed sample

Table 1 Characteristic parameters for the undeformed polymer

L	12.0 nm
$\langle \delta\rho_e^2 \rangle$	356 nm^{-6}
ϕ_c	0.26
d_c	3.5 nm
ρ_c	2.078×10^3 kg m^{-3}
ρ_a	1.945×10^3 kg m^{-3}

concentration fluctuations do not significantly contribute to the scattering of the terpolymer melt. The second term in equation (1) must therefore be attributed to the scattering from thermal density fluctuations provided crystallization of the material does not produce additional concentration fluctuations. After subtraction of the second term in equation (1), the first one has been analysed further to get information on the crystalline morphology of the material.

The invariant yields the mean-square electron density fluctuation $\langle \delta\rho_e^2 \rangle$, which results from the electron density difference between the crystalline and amorphous regions[26]:

$$(2\pi^2)^{-1} \int_0^\infty I(q) q^2 \mathrm{d}q = \langle \delta\rho_e^2 \rangle \qquad (3)$$

where $\delta\rho_e$ is the difference between the local electron density and the average taken over the whole sample volume. The value of $\langle \delta\rho_e^2 \rangle$ is indicated in *Table 1*. In the case of a two-phase system $\langle \delta\rho_e^2 \rangle$ is given by:

$$\langle \delta\rho_e^2 \rangle = (\rho_e^c - \rho_e^a)^2 \Phi_c (1 - \Phi_c) \qquad (4)$$

where ρ_e^c and ρ_e^a are the electron densities of the crystalline and amorphous regions, respectively, and Φ_c designates the volume fraction of the crystalline lamellae. The values of Φ_c and other morphological parameters such as the number average of the lamellar thickness d_c may be derived from the one-dimensional correlation function. This function normalized at $x = 0$ is given by:

$$\gamma(x) = (2\pi^2 \langle \delta\rho_e^2 \rangle)^{-1} \int_0^\infty I(q) q^2 \cos(qx) \mathrm{d}q \qquad (5)$$

Strobl and Schneider[28] demonstrated that Φ_c and d_c result from the 'self-correlation' triangle, which is constructed by extrapolation of the linear and horizontal sections of the correlation function. *Figure 8* shows the correlation function of the undeformed terpolymer. The straight section is well defined. However, the horizontal section degenerates to a minimum indicative of a broad distribution in lamellar thicknesses. To a first approximation, the baseline has been drawn through the minimum to obtain both Φ_c and d_c. The values calculated according to Strobl and Schneider are listed in *Table 1*.

The fact that Φ_c is more than twice as high as the crystallinity estimated from WAXS indicates that the stacks of lamellae are embedded in an amorphous matrix. This result is consistent with the highly distorted spherulitic superstructure revealed by small-angle light scattering. Inserting $\langle \rho_e^2 \rangle$ and Φ_c into equation (4) yields $\rho_e^c - \rho_e^a$. The value of $\rho_e^c - \rho_e^a$ may be converted into the difference in densities $\rho_c - \rho_a$ provided the distribution of the termonomer units in the crystalline and amorphous regions is known. The results of WAXS indicate the same type of molecular packing for the VDF/TFE/HFP terpolymer as observed for TFE. Several authors[20,29,30] have derived strong evidence that the HFP units are incorporated into the crytalline lattice of TFE. The assumption that the comonomer units are homogeneously distributed in the terpolymer yields $\rho_c - \rho_a$ and ρ_c from the SAXS and WAXS data, respectively. The values of ρ_c and ρ_a are included in *Table 1*.

The subsequent part focuses on the SAXS of samples that have been stretched to $\alpha = 4.5$ in the temperature range of 50–100°C. The intensive stress whitening of the terpolymer stretched at 20°C (see also the section headed 'Deformation behaviour') results in a strong equatorial scattering component, which precludes a detailed analysis of the fibre morphology. *Figure 9* shows the results of SAXS measurements conducted with point collimation and a two-dimensional detector. The four-point pattern changes to a two-point pattern when the drawing temperature increases. This result indicates that with increasing drawing temperature shear yielding produces stacks of lamellae whose surfaces are oriented normal to the draw axis. Quantitative information on the fibre morphology has been derived from measurements using a Kratky camera. *Figures 10* and *11* respectively show slit-smeared meridional and equatorial scattering curves. The long-period calculated from the position of the meridional scattering peak increases with drawing

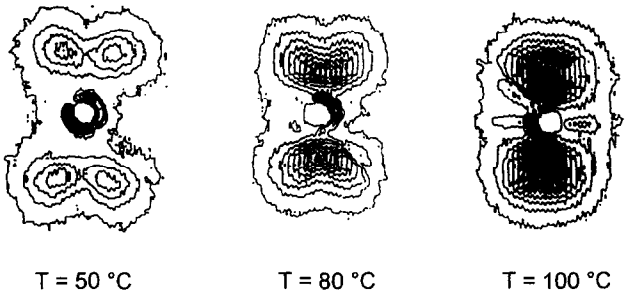

Figure 9 Effect of drawing temperature on the SAXS pattern of samples stretched to $\alpha \approx 4.5$

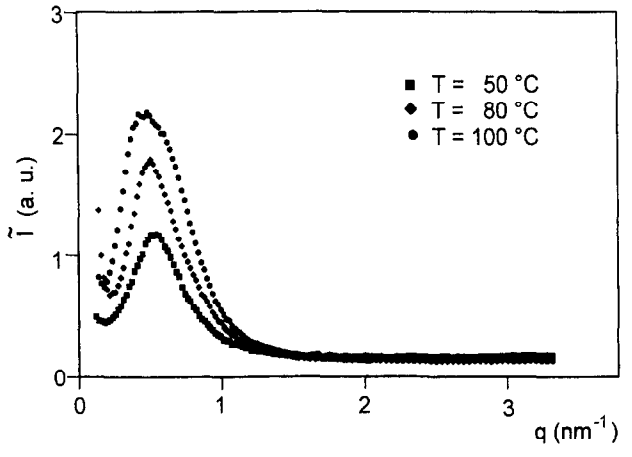

Figure 10 Slit-smeared SAXS curves of deformed samples ($\alpha \approx 4.5$) measured along the meridian. Parameter is the drawing temperature

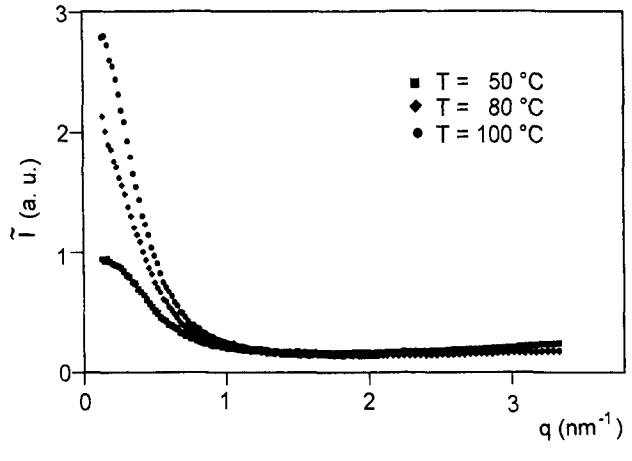

Figure 11 Slit-smeared SAXS curves of deformed samples ($\alpha \approx 4.5$) measured along the equator. Parameter is the drawing temperature

temperature (*Figure 12*). This effect must be attributed to the thermal treatment of the samples during the tensile test, which results in a partial melting of crystalline lamellae. In fact, the data for deformed samples compare well with those for undeformed samples submitted to the same thermal treatment (*Figure 12*). The invariant has been calculated from the equatorial scattering curves. For an oriented two-phase system with sharp phase boundaries and slit collimation, equations (1) and (2) may be written in the form[26]:

$$\tilde{I} = C/q_r^3 + D \tag{6}$$

$$\int_0^\infty \tilde{I}(q_r) q_r \, dq_r = K\langle \delta\rho_e^2 \rangle \tag{7}$$

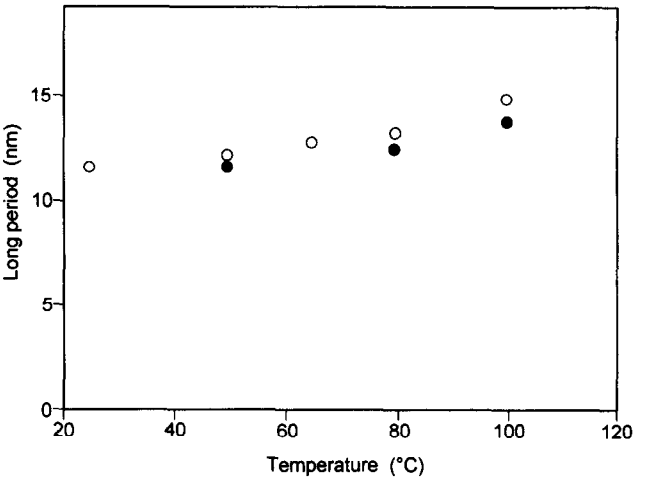

Figure 12 Long period as a function of annealing or drawing temperature: (○) undeformed samples and (●) samples stretched to $\alpha \approx 4.5$

where $\tilde{I}$ is the slit-smeared scattering intensity and q_r designates the equatorial component of the scattering vector. C, D and K are constants, which include geometrical parameters. Evaluation of the scattering data according to equation (6) did not reveal any significant effect of the orientation of the samples on the background scattering from thermal density fluctuations. After subtraction of the second term in equation (6), $\langle \delta\rho_e^2 \rangle$ has been calculated from equation (7) and plotted as a function of drawing temperature (*Figure 13*). It can be seen that $\langle \delta\rho_e^2 \rangle$ strongly decreases when the terpolymer is stretched at temperatures far below the melting point. With increasing drawing temperature, $\langle \delta\rho_e^2 \rangle$ approaches the value measured for undeformed samples. This is shown in *Figure 13*, where the data for deformed samples are compared to those for undeformed samples subjected to the same thermal treatment. According to equation (4), $\langle \delta\rho_e^2 \rangle$ is a function of ρ_e^c, ρ_e^a and Φ_c. Supplementary information is required to discuss the effect of drawing temperature on each of these parameters. The method of Strobl has been used to evaluate morphological parameters of the undeformed

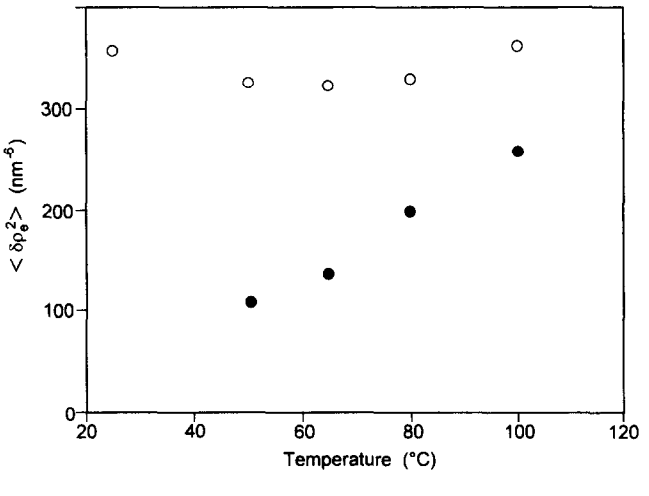

Figure 13 Mean-square fluctuation of the electron density as a function of annealing or drawing temperature: (○) undeformed samples and (●) samples stretched to $\alpha \approx 4.5$

material. Unfortunately, this method cannot be applied to slit-smeared scattering data of oriented systems without specific assumptions on the orientation distribution of the stacks of lamellae. Measurements performed with a density gradient column have shown that the effect of drawing on the density of the samples is within experimental error. This result is not surprising because of the low degree of crystallinity of the material. However, there is some evidence that ρ_c decreases with drawing temperature. In fact, unrealistic values of ρ_a and Φ_c must otherwise be assumed for the drawn material. The experimental results shown in *Figure 13* are in good agreement with those reported for polyethylene (PE) and poly(ethylene terephthalate) (PET) fibres. Fischer *et al.*[31,32] have demonstrated for these materials that ρ_c decreases with drawing or annealing temperature. They assumed that vacancies introduced near the grain boundaries reduce the density of the crystalline layers. Since the size of the mosaic blocks increases with drawing temperature, the number of vacancies becomes smaller and ρ_c approaches the value measured for the undrawn material.

CONCLUSIONS

Dynamical mechanical measurements have shown that the statistical VDF/TFE/HFP terpolymer exhibits two relaxation mechanisms, which are attributed to local and cooperative chain motions in the amorphous regions. The terpolymer is a ductile material that can be highly deformed in uniaxial tensile tests. The results of WAXS indicate that the crystalline structure of the terpolymer combines features of both VDF and TFE in agreement with previous studies of Lovinger *et al.*[5] on VDF/HFP copolymers. The incorporation of the HFP units strongly reduces the degree of crystallinity. SAXS experiments have clearly revealed the lamellar morphology of the material. Deformation of the terpolymer at low drawing temperatures, T, results in a four-point SAXS pattern that gradually changes to a two-point pattern when T increases. The long period increases slightly with T. This effect is attributed to a partial melting of crystalline lamellae. The mean-square fluctuation of the electron density $\langle \delta\rho_e^2 \rangle$ of samples stretched at low temperatures is considerably lower than that of undeformed samples. With increasing drawing temperature, $\langle \delta\rho_e^2 \rangle$ approaches the value measured for undeformed samples. To explain this effect, it is assumed that vacancies introduced near the grain boundaries reduce the density of the crystalline layers.

ACKNOWLEDGEMENTS

This work was supported by the Bundesministerium für Forschung und Technologie. One of the authors gratefully acknowledges funds from the Fonds der Chemischen Industrie. The material used in these studies was kindly provided by Dr Dittmer (Hoechst AG).

REFERENCES

1 Fitz, H. *Kunststoffe* 1987, **77,** 1016
2 Lovinger, A. J., Davies, G. T., Furukawa, T. and Broadhurst, M. G. *Macromolecules* 1982, **15,** 323
3 Lovinger, A. J., Furukawa, T., Davis, G. T. and Broadhurst, M. G. *Polymer* 1983, **24,** 1225
4 Lovinger, A. J. *Macromolecules* 1983, **16,** 1529
5 Lovinger, A. J., Davis, D. D., Cais, R. E. and Kometani, J. M. *Macromolecules* 1988, **21,** 78
6 Tatsaka, S. and Miyata, S. J. *J. Appl. Phys.* 1985, **57,** 906
7 Tashiro, K. and Kobayashi, M. *Polymer* 1986, **27,** 667
8 Bourgaux-Leonard, C., Legrand, J. F., Renault, A. and Delzenne, P. *Polymer* 1991, **32,** 597
9 Tashiro, K., Kaito, K. and Kobayashi, M. *Polymer* 1992, **3,** 2915
10 Bellet-Amalric, E., Legrand, J. F., Stock-Schweyer, M. and Meurer, B. *Polymer* 1994, **35,** 34
11 Lovinger, A. J. in 'Developments in Crystalline Polymers –1' (Ed D. C. Bassett), Applied Science, London, 1982, p. 195
12 McCrum, N. G. *Makromol. Chem.* 1959, **34,** 50
13 Eby, R. K. and Wilson, F. C. *J. Appl. Phys.* 1962, **33,** 2951
14 Moggi, G., Bonardelli, P. and Bart, J. C. J. *Polym. Bull.* 1982, **7,** 115
15 Gangal, S. V. in 'Encyclopedia of Polymer Science and Engineering' (Eds. H. F. Mark, N. M. Bikales, C. G. Overberger and G. Menges), Vol. 16, Wiley, New York, 1989, p. 601
16 Strobl, G. R. *Acta Crystallogr. (A)* 1970, **26,** 367
17 Yano, S. *J. Polym. Sci. (A-2)* 1970, **8,** 1057
18 McBrierty, V. J., Douglas, D. C. and Weber, T. A. *J. Polym. Sci., Polym. Phys. Edn.* 1976, **1,** 1271
19 Bunn, C. W. and Howells, E. R. *Nature* 1954, **17,** 549
20 Clark, E. S. and Muus, L. T. *Z. Krist.* 1962, **117,** 119
21 Corradini, P. and Guerra, G. *Macromolecules* 1977, **10,** 1410
22 Weeks, J. J., Eby, R. K. and Clark, E. S. *Polymer* 1981, **22,** 1496
23 Lando, J. B., Olf, H. G. and Peterlin, A. *J. Polym. Sci. (A)* 1966, **4,** 941
24 Moggi, G., Bonardelli, P. and Bart, J. C. *J. Polym. Sci., Polym. Phys. Edn.* 1984, **22,** 357
25 Lando, J. B. and Doll, W. W. *J. Macromol. Sci.–Phys. (B)* 1968, **2,** 205
26 Porod, G. *Kolloid Z.* 1951, **12,** 83
27 Wendorff, J. H. and Fischer, E. W. *Kolloid Z. Z. Polym.* 1973, **251,** 876
28 Strobl, G. R. and Schneider, M. *J. Polym. Sci., Polym. Phys. Edn.* 1980, **18,** 1343
29 Starkweather, H. W., Zoller, P. and Glover, A. *J. Polym. Sci., Polym. Phys. Edn.* 1984, **22,** 1431
30 Villani, V. and Puciariello, R. *Makromol. Chem.* 1990, **19,** 1143
31 Fischer, E. W., Goddar, H. and Schmidt, G. F. *J. Polym. Sci. (A)* 1969, **2,** 37
32 Fischer, E. W. and Fakirov, S. *J. Mater. Sci.* 1976, **11,** 1041